Journal of Infrastructure Intelligence and Resilience 2 (2023) 100051

Contents lists available at ScienceDirect

Journal of Infrastructure Intelligence and Resilience

journal homepage: www.journals.elsevier.com/journal-of-infrastructure-intelligence-and-resilience

Design and implementation of sustainable solar energy harvesting for low-cost remote sensors equipped with real-time monitoring systems

Kaveh Malek [a], Edgardo Ortíz Rodríguez [b], Yi-Chen Lee [c], Joshua Murillo [d,e], Ali Mohammadkhorasani [e], Lauren Vigil [e], Su Zhang [e,f], Fernando Moreu [e,*]

[a] Department of Mechanical Engineering, University of New Mexico (UNM), Albuquerque, NM 87131, USA
[b] Electrical Engineering Department, Ana G Mendez Gurabo Campus, Puerto Rico
[c] Civil Engineering Department and Bio-Environmental Engineering Department, National Taiwan University, Taiwan, China
[d] Global and National Security Policy Institute, University of New Mexico (UNM), Albuquerque, NM 87131, USA
[e] Department of Civil, Construction, and Environmental Engineering, University of New Mexico (UNM), Albuquerque, NM 87131, USA
[f] Earth Data Analysis Center (EDAC), University of New Mexico (UNM), Albuquerque, NM 87131, USA

ARTICLE INFO

Keywords:
Solar energy harvesting
Low-cost
Real time monitoring
Wireless smart sensor networks

ABSTRACT

Data acquisition systems, such as Wireless Smart Sensor Networks (WSSNs) can increase the resilience of infrastructure by providing real-time monitoring and data collection of environmental parameters. Yet, sustainable energy supplies for sensor networks established in remote and inaccessible areas still present a challenge. Previously, researchers have attempted to address this difficulty by proposing different energy systems including solar energy harvesting, however, significant prolonged experimental data for the operation of extensive networks powered by solar energy has not been reported. This paper presents an original design and implementation of an energy system for a large WSSN and provides the sensors' power status data over a significant duration. A network of low-cost flood monitoring sensors, including twenty-six water level sensors, twenty rain gauges, and eight communication nodes were deployed and tested on summer and fall 2022 at six remote locations at the northern New Mexico Pueblo, Ohkay Owingeh. A thermometer and a humidity sensor were added to each communication node to record temperature and air's moisture level. In addition, a networked voltage monitoring system was deployed to observe the sensors energy status in real-time. The items of the WSSN are composed of two differing energy circuits suited for their energy demands. The sensors' energy circuits contain a photovoltaic panel, a lithium-polymer battery, a control device, and a DC-to-DC converter. Whereas the communication nodes contain another photovoltaic panel, a lead-acid battery, and a solar charging controller. The findings provide a perspective on the long-term field deployment of WSSNs consisting of low-cost sensors.

1. Introduction

WSSNs can be grouped under the intelligent methods for ensuring resilience of infrastructure because they leverage advanced technologies such as wireless communication, sensing, and data analytics to enhance the resilience of critical infrastructure systems (Mottahedi et al., 2021; Ma et al., 2023). WSSNs can provide real-time data on the health and performance of various components of infrastructure, enabling proactive maintenance and reducing downtime (Guo et al., 2021). Real-time data acquisition via multifunctional sensor nodes and wireless networks is made possible by recent technological advancements in digital electronics, wireless technologies, and the expansion of internet connectivity (Shanmuganthan et al., 2008).

Although several brands have produced commercial systems for the collection of infrastructure data, their products are costly, limited to certain atmospheric measurements, and usually dependent on an exclusive manufacturer's platform for implementation (Botero-Valencia et al., 2022). Additionally, these products often need technical expertise for setup or maintenance, in addition to extensive wiring for power, making their deployment difficult in inaccessible regions(Khandelwal and Singhal, 2021). The aforementioned limitations of commercial sensors and the significant implications for efficient data collection has

* Corresponding author. Room 3056 Centennial Engineering Center, The University of New Mexico, Albuquerque, NM 87131, USA.
E-mail address: fmoreu@unm.edu (F. Moreu).

https://doi.org/10.1016/j.iintel.2023.100051
Received 21 March 2023; Received in revised form 15 July 2023; Accepted 18 July 2023
Available online 22 July 2023
2772-9915/© 2023 The Authors. Published by Elsevier Ltd on behalf of Zhejiang University and Zhejiang University Press Co., Ltd. This is an open access article under the CC BY-NC-ND license (http://creativecommons.org/licenses/by-nc-nd/4.0/).

Table 1
Several aspects of experimental studies on solar-powered WSSN.

Ref.	Processor	Sensor Type	Deployment Location	Period	Sensors# Analyzed in the Study	Solar-Powered Communication
Dutta et al. (2006)	MSP430	NM	Remote location	Less than 1 day	557	Solar-powered gateway
Corke et al. (2007)	At-mega 128	NM	Work site	365 days	1	No
Barrenetxea et al. (2008)	MSP430	Wind speed/ direction	Remote location	30 days	18	No
(Dehwah et al., 2015)	Libelium Waspmote	NM	Urban setting	14 days	4	No
Ma et al. (2022)	ACS300-MM	Wind speed/ direction	Solar power plant	1 day	1	Solar-powered D3G7M5
(Xiao et al., 2023)	ESP8266 MCU	Temperature/ humidity	Indoor lab (outdoor solar panel)	Less than 1 day	1	No

*NM: not mentioned in the paper.

prompted the design of low-cost self-made sensors (Botero-Valencia et al., 2022). The studies and developments on this sensor type is exponentially increasing due to their unparalleled data to cost ratio that makes it possible to inexpensively conduct research in a variety of fields and applications (Ozdagli et al., 2018; Mao et al., 2019).

Energy consumption is a significant design factor which influences the lifespan of low-cost self-made WSSNs and the amount of data they collect in outdoor applications, particularly in hard-to-access locations (Nsabagwa et al., 2019). Two sustainable resources for powering sensor nodes are transferred energy and renewable energy (Akhtar and Rehmani, 2015). The transferred energy research includes, but is not limited to, inductive coupling (LaMarca et al., 2002; Andringa et al., 2005; Yao et al., 2006), laser (Afzal et al., 2008), and acoustic emission (Denisov and Yeatman, 2010; Ozeri and Shmilovitz, 2010). On the other hand, renewable energy studies have focused on wind (Weimer et al., 2006; Shen et al., 2008; Sardini and Serpelloni, 2011), piezoelectric conversion of environmental energy (Roundy and Wright, 2004; Wang and Song, 2006; Goudar et al., 2014), and solar energy.

Solar energy studies constitute most research on the renewable power generation for WSSNs. Several studies conducted numerical or analytical simulation to evaluate the level of boost in WSSN lifetime when the sensors are equipped with a solar system (Simjee and Chou, 2006; Jackson et al., 2017; Sharma et al., 2018; Wang et al., 2017; Yang et al., 2020; Getahun et al., 2022; Mansura et al., 2022; Wan and Chen, 2022). While these simulation-based approaches provide valuable insights, experimental investigations are crucial for understanding the true impact of implementing solar systems in WSSN sensors.

Table 1 summarizes several aspects presented in the experimental efforts shown in the first column. The processors and type of sensors are shown in the second and third columns, respectively. The deployment locations encompass remote areas, work sites, urban settings, solar power plants, and indoor labs (fourth column). However, an analysis of the literature reveals a significant research gap: most of these experimental studies have either employed a limited number of sensor nodes or restricted their analysis period to 1 day or less (columns five and six). This scarcity of long-term experimental data regarding the deployment of numerous sensors in remote locations highlights the need for further research in this area. Moreover, although one study (Barrenetxea et al., 2008) deployed a substantial number of sensors over an extended period, it is important to note that their communication gateway was not solar-powered (column seven). The finding of Table 1 underscores the lack of reports documenting large-scale sensor networks fully powered by solar energy.

Reporting deployment data of sizable WSSNs over long periods is essential for several reasons. First, it allows for an assessment of the disparity between theoretical expectations and real-world performance of WSSNs powered by solar energy. Second, it provides an insight into the repeatability and reliability of self-made sensor networks. Finally, the availability of experimental data serves as a foundation for validating simulation methods.

This study addresses this research gap by providing experimental data on the deployment of a solar-powered WSSN while investigating the specific challenge of sustainable energy supplies for WSSNs deployed in remote areas. The hypothesis is that the voltage of designed sensor and communication nodes that are successfully tested in laboratory, will overall show a sustainable trend of variation during deployment despite some underperformances stemming from unpredicted field events. The research team employs an experimental methodology and implements a prolonged field deployment of large solar-powered WSSNs consisting of affordable sensors to assess this hypothesis. More specifically, a network of low-cost flood monitoring sensors including twenty-six water level sensors, twenty rain gauges, and eight communication nodes is deployed

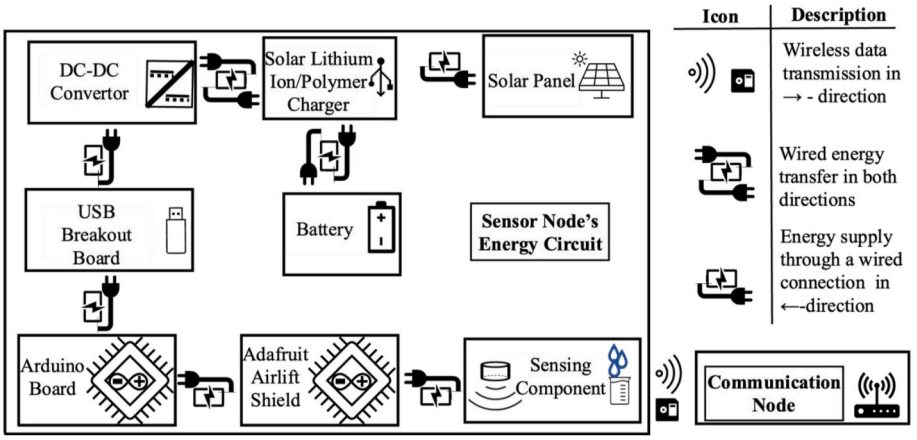

Fig. 1. Outline of the energy circuit for a sensor.

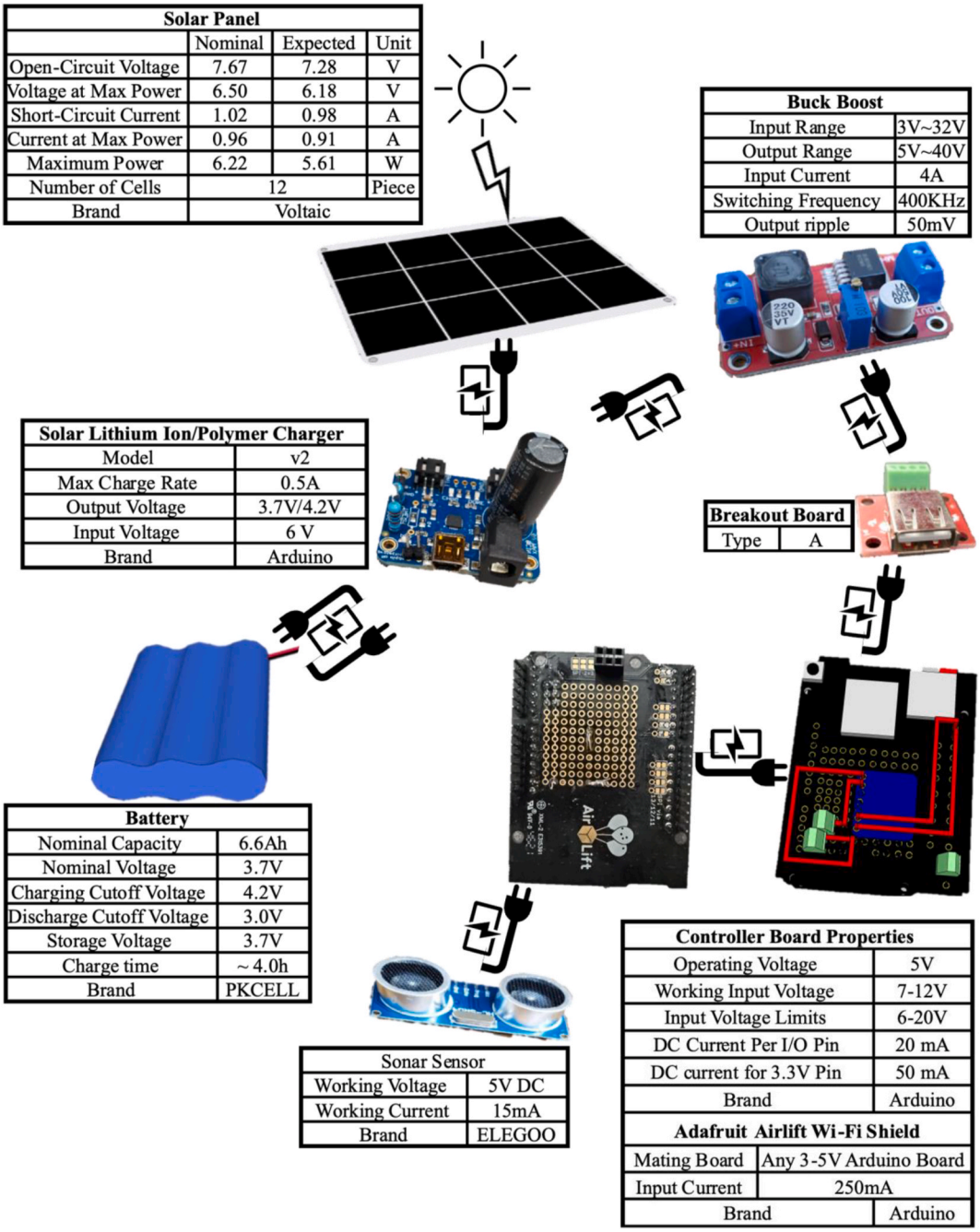

Fig. 2. Components of the energy circuit of the sensor nodes (sonar sensor) and their specifications.

in the vast remote area of the New Mexico Pueblo of Ohkay Owingeh during summer and fall 2022. The data of these fifty-four sensors are presented and analyzed for one month in this paper. Additionally, the design and manufacturing of the sensor networks are discussed in this paper. Furthermore, a monitoring strategy is developed to ensure the robust operation of the deployed sensor network. The interface enables real-time monitoring and reporting of the sensor circuits' voltages during the deployment, setting maintenance intervals, and enhancing the overall sustainability of the method.

2. Energy harvesting system

This section describes the components, design, and implementation of the energy harvesting system for the low-cost remote sensors equipped with real-time monitoring systems. The system's two main components, namely sensor nodes and communication nodes are discussed separately in this section.

2.1. Energy circuit of sensor nodes

To explore the energy circuit for the sensor nodes, a general description of the energy unit is initially provided. The main components and the drawing of the energy circuit are then described. Finally, the basic calculation and the protype design and evaluation are explained.

2.1.1. Outline of the circuit

Fig. 1 shows the connection between the basic components of the sensor node's energy circuit. A photovoltaic panel collects solar energy during daytime and charges a lithium polymer battery while also

powering a microcontroller through a DC-DC converter. The DC-DC converter boosts the DC voltage received from the panel to the degree required to operate of the Arduino Uno board. The battery in this system reserves solar energy during the day and automatically powers the circuit during the nights or temporary shades for transmission of the data collected. Additionally, an on-board ESP32 chip that is attached on top of the Airlift Shield provides the necessary wireless capabilities.

2.1.2. Circuit components and diagram

Fig. 2 schematically describes the components of the sonar sensor node's energy circuit with their specifications. The process of selecting these components is described in section 2.1.3. Fig. 3 shows the circuit diagram of this node. A 6.22W 6.5V solar panel is connected to a solar lithium-ion charger including a 4.7F capacitor and a mcp73871 microchip for voltage regulation. This charger establishes a bidirectional and unidirectional energy transfer with a 3.7V lithium-polymer battery and a DC-DC converter, respectively. On a sunny day, the solar panel charges the battery and supplies input to the converter at a voltage range of 6V–6.5V. The DC-DC converter then bucks the output voltage to 5.4V–5.6V. At night, the battery supplies the input of the converter at a voltage range of 3.2V–4.2V. The converter boosts the voltage to 5.2V–5.5V. This output range of converter's voltage safely operates the Arduino which functions on 5V logic. Two main components attached to the Arduino boards are a sensor and the Airlift Shield with an on-board ESP32 chip providing wireless capabilities. The on-board ESP32 is integrated into the Arduino Wi-Fi shield and is not shown as a separate component in the circuit. The sonar sensor is connected to the Arduino through a ground pin, a 5V power pin, and 2 digital Input/Output (I/O) pins. These digital pins (D2 and D3 in Fig. 3) can be replaced with other digital pins through the code. The circuit diagram of rain sensors is similar to sonar sensors' diagram and therefore is not shown in this section. The only difference between the circuit diagram of rain sensors with Fig. 3 is the connection between Arduino board and the sensor. The rain sensors have the same power input and ground connection pins as sonar sensors, but only one digital pin (D3) is used for data transmission as opposed to the two digital pins in sonar sensors (D2 and D3).

2.1.3. Calculations and prototype evaluation

The panel size is assessed based on the ratio of the yearly peak sun hour and energy consumption. The yearly peak sun hour for a south-facing flat-plate collector at a fixed tilt is 5.6 kW h/m2/day in New Mexico (Dunlap et al., 1994). The power consumption is empirically measured using a multimeter from which the annual energy consumption of a node is estimated at 6861.1W.hr for sonar sensor. Selecting a typical derate factor equal to 0.77 approximates various losses and inefficiencies in the PV system components (Marion et al., 2005). A conservative shade factor of 0.7 is applied to the default derate factor decreasing it to 0.54. Annual energy required by the solar panel is:

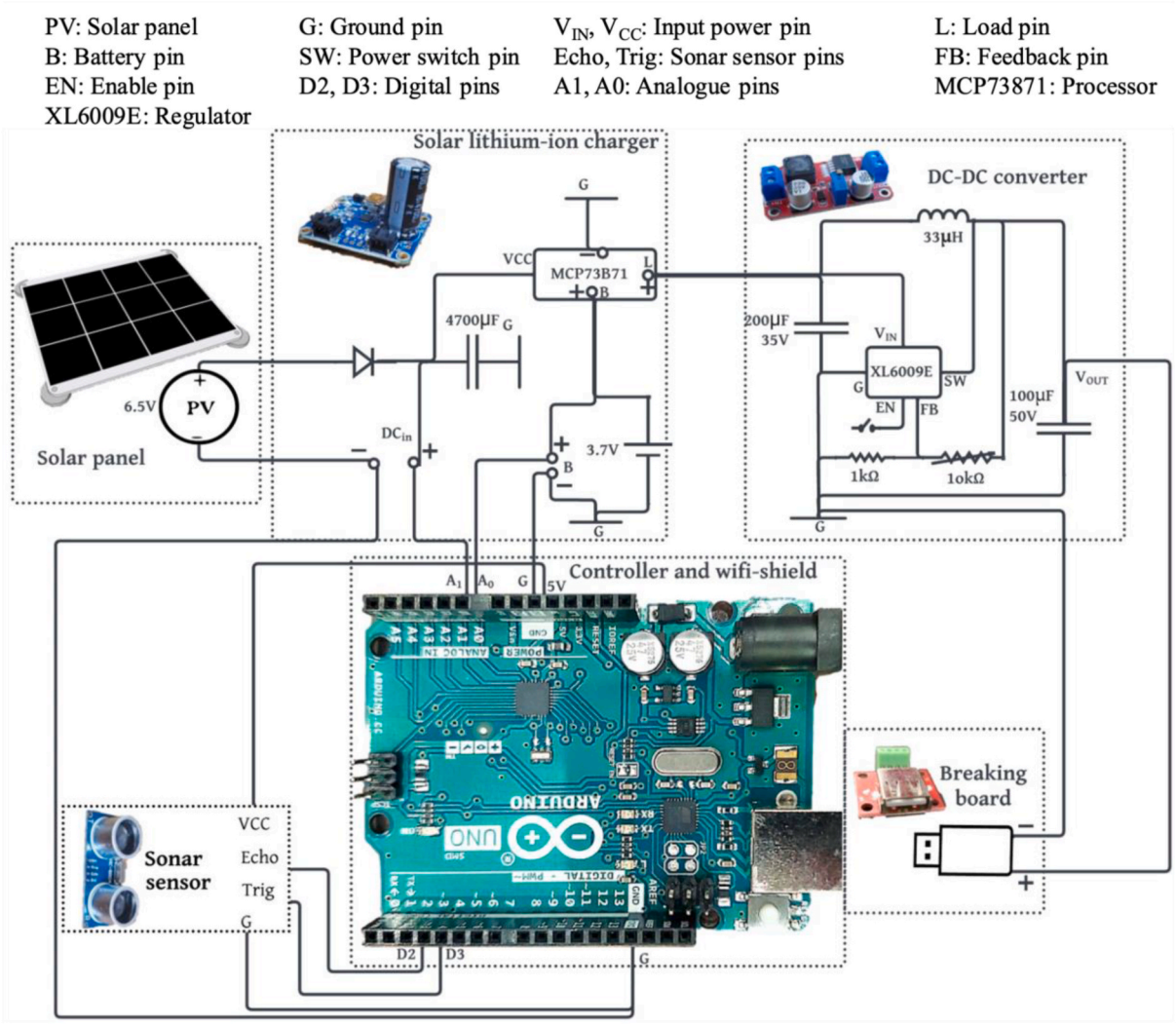

Fig. 3. Circuit diagram of the energy unit for a sonar sensor node.

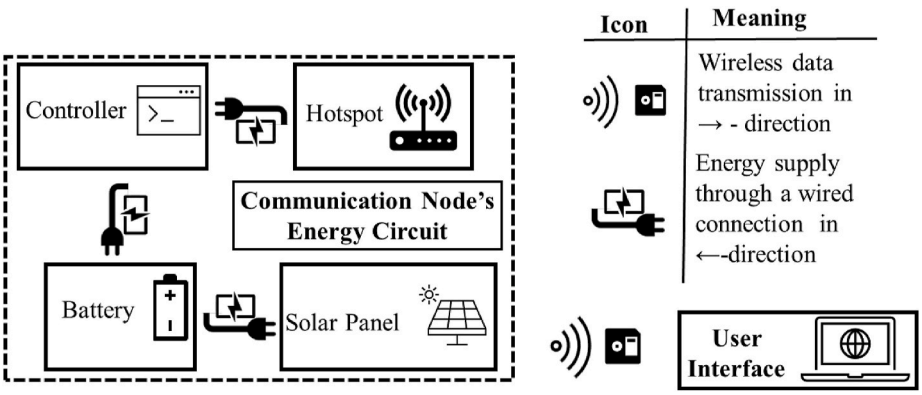

Fig. 4. Outline of the energy unit for a communication node.

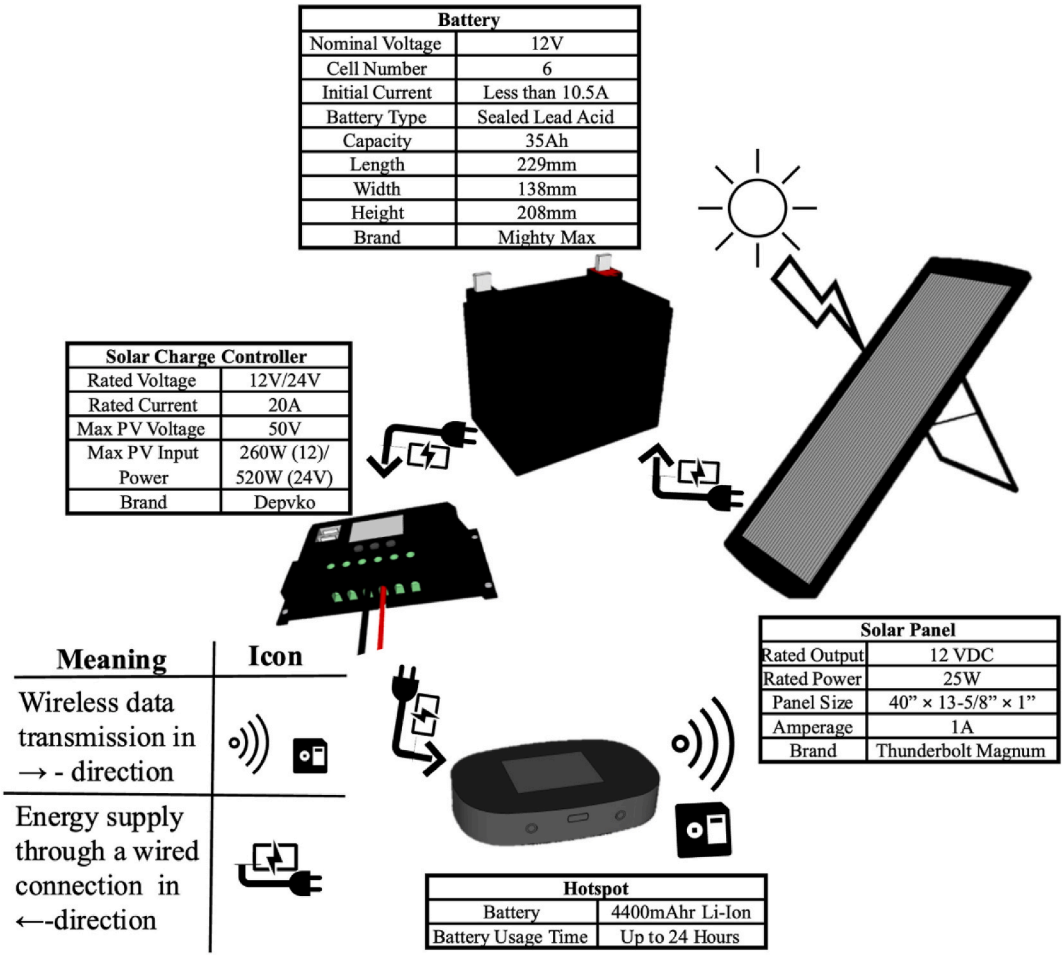

Fig. 5. Components of communication nodes' energy circuit with specifications.

$$Anual\ required\ energy = \frac{anual\ energy\ consumed\ by\ loads}{solar\ panel\ derate\ factors} = \frac{6861.1\text{W.hr}}{0.54} = 12705.7\text{W.hr}$$

$$Solar\ panel's\ power = \frac{anual\ required\ energy}{annual\ peak\ sun\ hour} = \frac{12705.7\text{W.hr}}{\frac{5.6\times1000\frac{\text{W.hr}}{\text{m}^2.\text{days}}\times365days}{1000\frac{\text{W}}{\text{m}^2}}} = 6.2W$$

The battery's capacity is analyzed based on the daily load of the sensor for one day of autonomy during summer. Additionally, the Depth of Discharge (DoD) for each lithium-ion polymer battery is considered 85%. The daily load of a sonar sensor is experimental evaluated at

$$Daily\ load = \frac{annual\ load}{days\ in\ a\ year} = \frac{6861.1}{365} = 18.79W.hr$$

And the subsystem losses includes:
Wiring losses: 97% (Marion et al., 2005)
Conversion efficiency: 92% (Marion et al., 2005)
Round-trip efficiency 95% (Li, 2008).

Value of 77% has been chosen to account for the battery capacity drop at lower temperatures (when the ambient temperature drops to −15 °C from the battery test temperature) (Aris and Shabani, 2017).

$$Battery\ capacity = \frac{daily\ electric\ load \times days\ of\ autonomy \times temperature\ conversion\ factor}{voltage \times load\ subsystem\ efficiency \times depth\ of\ discharge} = \frac{18.79 \times 1 \times 1.23}{5 \times 0.95 \times 0.97 \times 0.92 \times 0.85} = 6.3A.hr$$

After selecting the battery and the solar panels based on the results of calculations, the researchers selected the other components of sensor node's energy circuit, based on the consistency of electrical characteristics of the connected components also considering that the sonar sensors are fed with 5V input. Next, the researchers tested and evaluated the sustainability and performance for a prototype using a seven-day running-test in summer in the actual environmental conditions they would be deployed in.

The battery's capacity is assessed based on the sensor's daily load for one day of autonomy during summer. A 60% Depth of Discharge (DoD) is considered for each lead-acid battery. The daily load of a sonar sensor is experimentally determined as 66W.hr. Subsystem losses include wiring losses (97%), conversion efficiency (92%), and round-trip efficiency (95%). A value of 77% is chosen for the battery capacity drop at lower temperature.

$$Battery\ capacity = \frac{daily\ electric\ load \times days\ of\ autonomy \times temperature\ conversion\ factor}{voltage \times load\ subsystem\ efficiency \times depth\ of\ discharge} = \frac{66 \times 1 \times 1.23}{5 \times 0.95 \times 0.97 \times 0.92 \times 0.6} = 31.9A.hr$$

2.2. Energy circuit of communication nodes

The exploration of the communication nodes' energy circuit begins with an initial description of the energy unit. This is followed by a detailed explanation of the main components comprising the energy circuit. Lastly, the basic calculation of the energy unit is outlined.

2.2.1. Outline and components of the circuit

Fig. 4 shows the basic components of the communication node's energy circuit and their connections. Fig. 5 provides the specifications and demonstrates the schematic illustration of the components of the communication node's energy circuit. During sun hours, solar energy is captured by a 25W solar panel to fill a 12V lead-acid battery that powers a portable hotspot with a 4400 mA h lithium-ion battery. The hotspot connects to a 12V/24V-20A charge controller through which it receives the battery's electricity. The benefits of the charge controller include (LokeshReddy et al., 2017): (1) optimizing the transferred power by adapting the circuit's operation at maximum power point regardless of variations in irradiation (2) shortening the charging time (3) increasing the battery's life by preventing excessive charge and discharge. Overall, the circuit provides efficient and sustainable energy harvesting power for the unit that provides continuous online connectivity to its respective sensors.

2.2.2. Calculations and prototype assessment

The panel size is determined by the ratio of the yearly peak sun hour and energy consumption. In New Mexico, the peak sun hour is 6.2 kW h/m2/day for a 45° flat-plate collector (Dunlap et al., 1994). The measured energy consumption of a hotspot is 8030W.hr during a year, and each communication node supports up to three hotspots. A derate factor of 0.54 is applied to account for system losses and shading as described in section 2.1.3. The annual energy required by the solar panel is calculated accordingly:

$$Anual\ required\ energy = \frac{anual\ energy\ consumed\ by\ loads}{solar\ panel\ derate\ factors} = \frac{24090\ \text{W.hr}}{0.54} = 44611.1\ \text{W.hr}$$

$$Solar\ panel's\ power = \frac{anual\ required\ energy}{annual\ peak\ sun\ hour} = \frac{44611.1\ \text{W.hr}}{\frac{6.2 \times 1000\ \frac{\text{W.hr}}{\text{m}^2\text{.days}} \times 365 days}{1000\ \frac{\text{W}}{\text{m}^2}}} = 19.7W$$

The researchers chose the parts of the communication node's energy circuit and checked that all connected components had consistent electrical characteristics. They then conducted a seven-day test during summer to assess the durability and performance of a prototype under real environmental conditions.

3. Implemented WSSN

This research implements a low-cost sensor network run by the proposed power architecture to evaluate the performance of the energy system. The network consists of various components, including sensors, communication nodes, and auxiliary systems. This section provides an overview of the WSSN, discusses its different components, and explores field deployment of the components of the WSSN.

3.1. WSSN outline

Fig. 6 shows the basic blocks and connections of the sensor nodes, the communication nodes, and the user interface of the implemented network. The process proceeds with sensors collecting data of precipitation and water level then, transmitting the data to the communication nodes. These communication nodes are hand-held hotspots, which enable a connection from the sensors to a database that permanently stores the data collected. The database then relays the data to the Graphic User Interface (GUI) of the network; a website where the data are plotted and presented in final format.

3.2. Sensors description

The network of low-cost sensors involved in this study is comprised of twenty rain gauges and twenty-six water level sensors positioned in six different places. Fig. 7a provides a schematic illustration of rain gauges. This study uses WH-SP-RG rain gauges from the manufacturer MISOL. These gauges have a tilting mechanism that includes a rainwater collector, a funnel, a tipping lever, a tipping bucket, and reed switches (Savina et al., 2012). The rainfall is collected inside the collector and channeled through the funnel toward the tipping buckets. Each bucket's tip is approximately equivalent to 0.28 mm of rainfall, and once the tip occurs it creates momentary contact closure with its respective reed switch that is recorded via an interrupt pin signal (www.misolie.net, 2022). Fig. 7b exhibits the schematic illustration of the water level sensors and exhibits the box encompassing the electrical assembly of

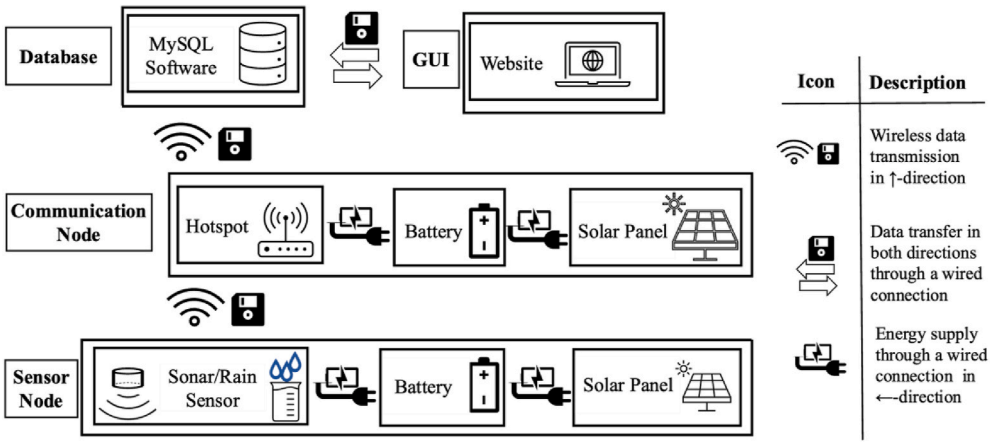

Fig. 6. Outline of the sensor network and its elements with their energy units.

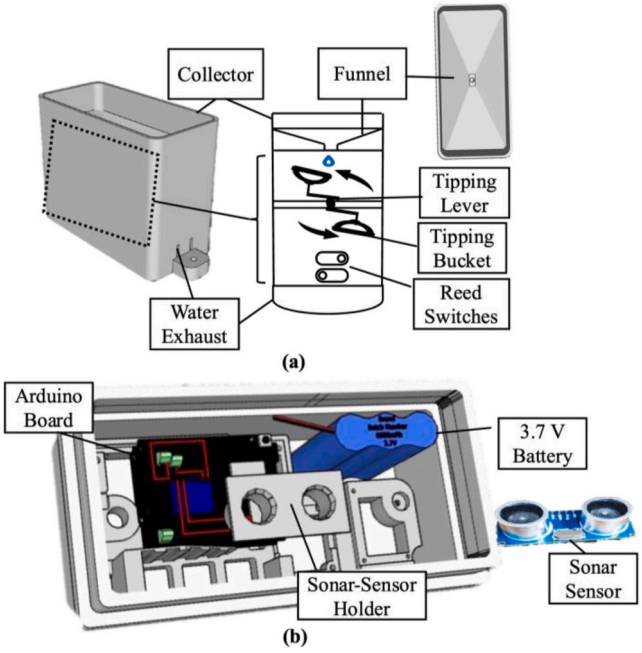

Fig. 7. Illustration of sensors (a) rain gauge (b) water level sensor.

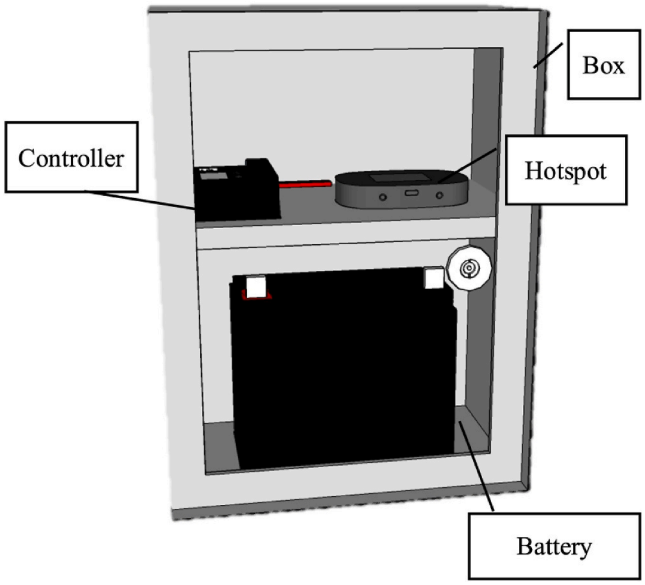

Fig. 8. Illustration of the communication nodes.

Table 2
Sonar component specifications.

Brand	ELEGOO
Model	HC-SR04
Max Range	500 cm
Min Range	2 cm
Measuring Angle	15°

both sensors. The ultrasonic measuring component is mounted via a 3D printed sonar holder to an ABS plastic junction box then connected to an Arduino board powered by a 3.7V lithium polymer battery circuit. Table 2 shows the specifications of the sonar component used in the deployment.The prospect of using rain and sonar sensors is to improve flood prediction in waterways. Flooding is one the five extreme events (Naser, 2023) that poses a significant threat to social stability and economic growth in regions prone to floods (Naseri and Hummel, 2021). The data required for flood prediction is usually collected inaccessible off-grid areas (Zakaria et al., 2023). The rain sensors are used to measure

Table 3
Hotspot communication node specification.

Brand	MiFi
Wireless Technology	Global Cat 9 LTE HSPA+/UMTS/EDGE/GPRS, 1x/EV-DO
Max Theoretical Download Speed	450Mbps
Wi-Fi Version	802.11 b/g/n/ac
Max Connection	Up to 15 Device
Security Features	Wi-Fi Security (WPA/WPA2) Wi-Fi Protected Setups (WPS) Wi-Fi Privacy Separation
System Support	Windows 7, 8, 10 Mac OS 10.7 or Higher Linux Ubuntu 12.4 or Higher
Wi-fi Bands	2.4 GHz and 5 GHz Simultaneous
Dimensions	109 × 67 × 18 mm
Weight	152 gr
Operating Temperature	−10 °C–55 °C

Fig. 9. Graphic of the auxiliary elements (a) sensor stand (b) sign.

Table 4
Total cost of the main components of sensor and communication nodes.

Items	Prices	Links
Sensor Solar Panel	$69.00	https://www.adafruit.com/product/1525
Buck Boost	$1.84	https://www.amazon.com/HiLetgo-Adjustable-DC3-0-30V-DC5-35V-Converter/dp/B00LP2LZ4M
Solar Lithium Ion/ Polymer Charger	$17.50	https://www.adafruit.com/product/390
Arduino UNO R3	$26.79	https://www.amazon.com/Arduino-A000066-ARDUINO-UNO-R3/dp/B008GRTSV6
Sonar Sensor	$12.99	https://www.amazon.com/ELEGOO-HC-SR04-Ultrasonic-Distance-MEGA2560/dp/B01COSN7O6
Sensor Battery	$24.50	https://www.adafruit.com/product/353
Communication Node's Solar Panel	$69.99	https://www.harborfreight.com/25-W-solar-panel-63940.html?utm_source
Communication Node's Battery	$69.99	https://www.amazon.com/ML35-12-Battery-Mighty-Brand-Product/dp/B00K8V2VD0
Solar Charger Controller	$14.92	https://www.amazon.com/Controller-Intelligent-Regulator-Paremeter-Adjustable/dp/B08L8TBCK6
Hotspot	$149.03	https://www.amazon.com/Verizon-Jetpack-Hotspot-WiFi-Device/dp/B09LYMZ49Q/ref
Wi-Fi shield	$14.95	https://www.adafruit.com/product/4285
Total Cost	$471.50	

the intensity and duration of rainfall in real-time, which is a critical factor in determining the likelihood and severity of flooding. The sonar sensors, on the other hand, are used to measure water levels and the flow rate of water in the waterways. Combining the data from the rain and sonar sensors will potentiate developing flood prediction models that can provide early warnings and help mitigate the damage caused by flooding.

3.3. Deployed communication nodes

In conjunction with every three sensors deployed, a communication node is attached providing them internet connection; amounting to a total of 8 for the network studied. These communication nodes are schematically illustrated in Fig. 8, showing the main component being a mobile hotspot that receives and transmits data from sensor to the server. The other components are composed of an energy circuit, which contains a solar charging controller that directs collected energy to provide a constant charge to the hotspot and provides external protection of the internal electrical devices during long term outdoor operation. Table 3 provides the specifications of the hotspot such as its dimensions, weight, operating temperature, security features, maximum possible connections, supported operating systems, and theoretical download speed.

3.4. Auxiliaries

Several auxiliary elements such as sensor stands, fasteners, and signs are required for sensor deployment. The schematic illustration of the sensor stands, and signs used in this study are presented in Fig. 9. The stand is one of the installation methods used to fix the sensors in their locations of operation. The final designs of the stands, such as the shape and dimension of the seat depend on the combination of the sensors installed on them. The sign gives a friendly message about the significance of the sensor network for the local community in English and Tewa (Ohkay Owingeh Pueblo's native languages).

3.5. Total cost of system

The cost of the major components of the sensors and communication nodes for small-scale production are listed in Table 4. The purchase link for each item is also provided in a separate column in the table. The total cost of the main components of a sensor node and a communication node are $152.62 and $303.93, respectively. Each communication node can handle connectivity and data transfer for up to fifteen sensors which can decrease the costs of a network depending on the configuration desired.

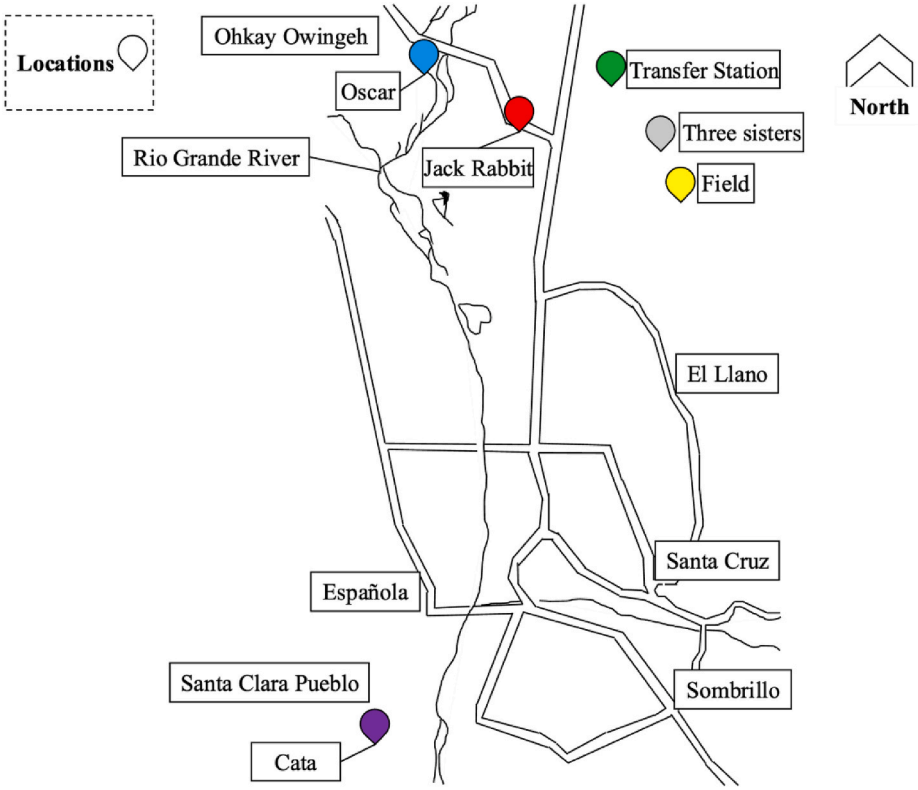

Fig. 10. Deployment locations.

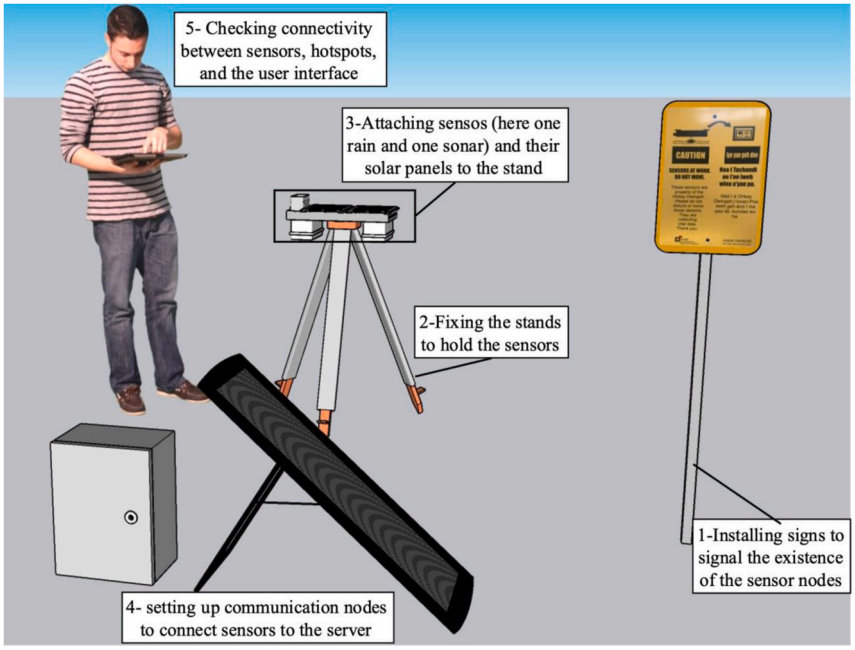

Fig. 11. Sensor deployment steps.

Low-cost WSSN is a widely-proposed solution to large-scale automation and data-acquisition systems such as ocean of things (Waterston et al., 2019) and smart cities (Candia et al., 2018). The cost-efficient nature of these components allows for a more accessible and scalable deployment, enabling a larger number of sensors to be integrated into the network within the available budget. This increased sensor density enhances data collection capabilities and improves the spatial coverage of the network (Karagulian et al., 2019).

3.6. Deployment

To validate the energy system in a real-world field application, the researchers deployed the sensors in six uncultivated lands within the northern pueblo of Ohkay Owingeh, New Mexico, USA. Fig. 10 provides the map and designation of the deployment locations. The research team monitored the performance of the networks' energy systems in these locations from May 1st, 2022, to November 1st, 2022.

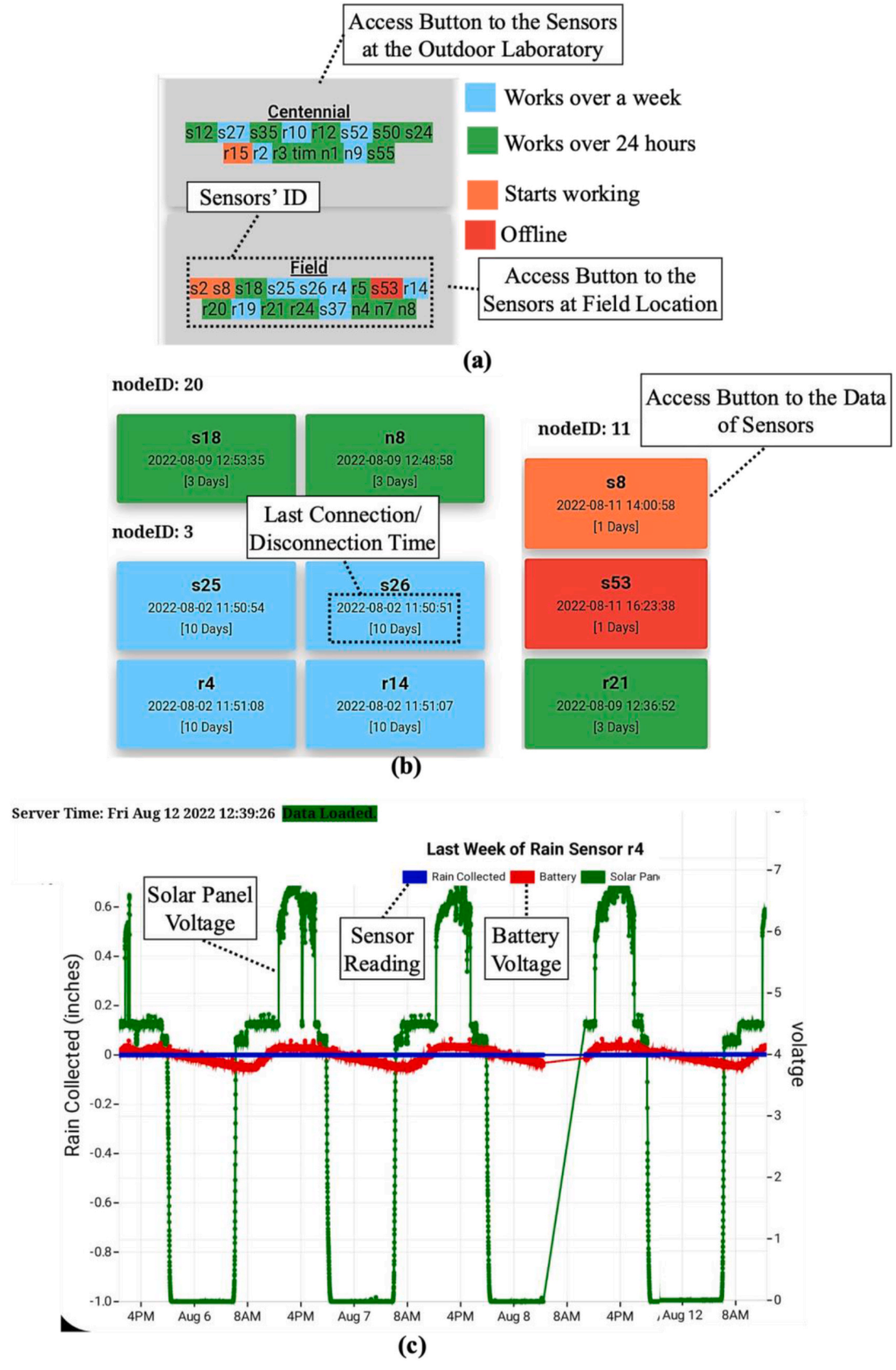

Fig. 12. Developed user interface, (a) homepage (b) the Field location (c) r4 sensor page example.

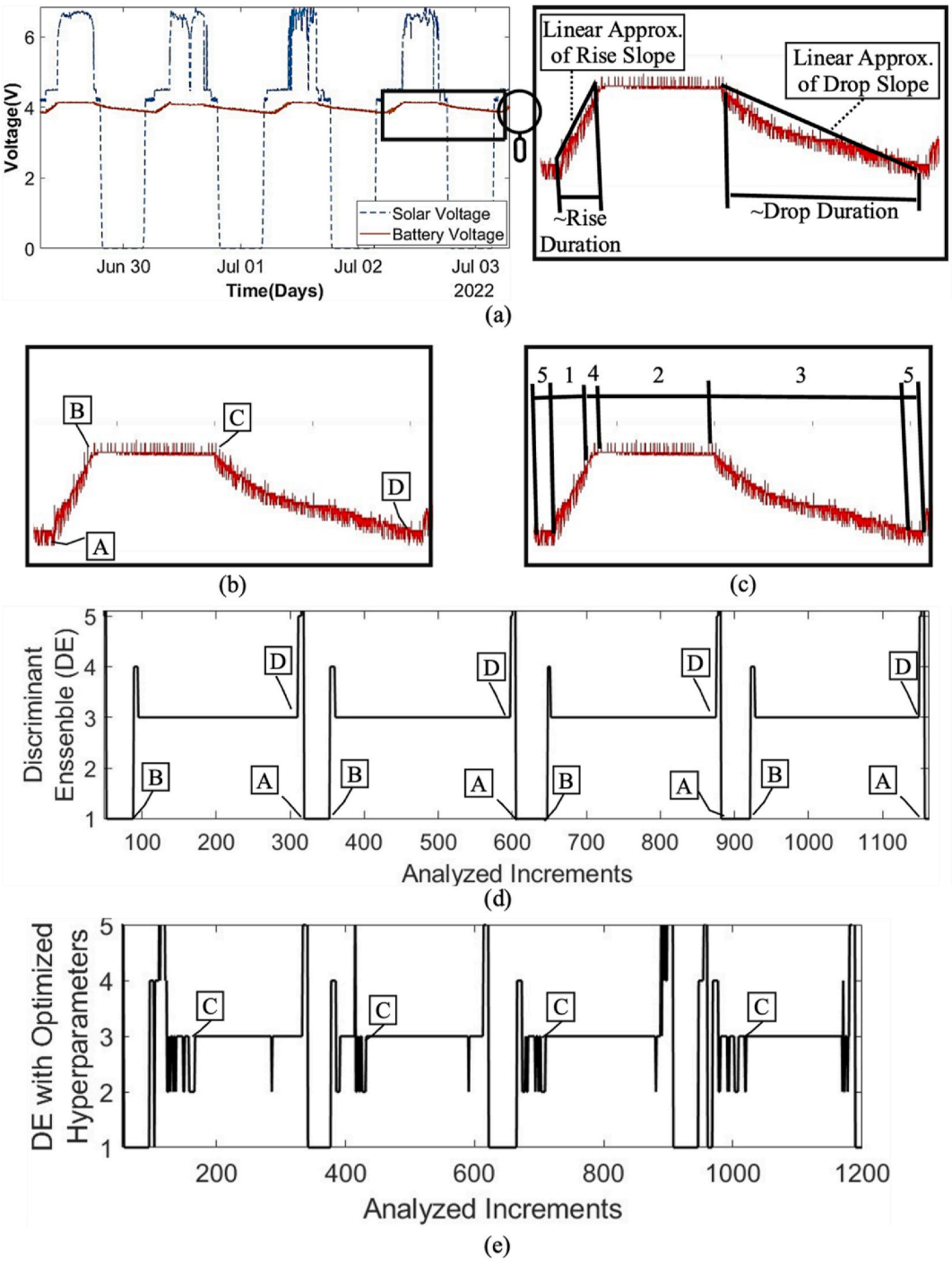

Fig. 13. Voltage evaluation method, (a) voltage graph example with slope and duration demonstration (b) start and end of charge/discharge process (c) five classes used in the ML model (d) ensembles of discriminant classifiers (e) ensembles of discriminant classifiers with optimized hyper parameters.

3.6.1. Deployment preparation

The research team manufactured, calibrated, and tested the sensors inside a laboratory at the UNM Center for Advanced Research Computing (CARC) prior to their consideration for field deployment. The voltages of sensors' batteries were first verified, having the required criteria of being capable of maintaining a voltage of 4.1 V. Additionally, the adequacy of all hotspots' batteries regarding their voltages was verified where batteries with less than 90% charge were recharged. Prior to each deployment the researchers installed the sensors at an outdoor laboratory a part of UNM Centennial Engineering Center, as a means of providing operation conditions similar to those of the field for a minimum of five days. The sensors that operated uninterruptedly at this test were qualified for deployment and were packaged for the following field trip. The other sensors which do not meet the criterion were transferred to the manufacturing laboratory to undergo a troubleshooting process.

3.6.2. Deployment process

The deployment process included: (1) transferring the qualified sensors, hotspots, energy devices, and the auxiliary parts to the planned locations, (2) installing the devices in the field, (3) establishing the required connections between sensor nodes, communication nodes, and the user interface, and (4) verifying the operation of the sensors on the

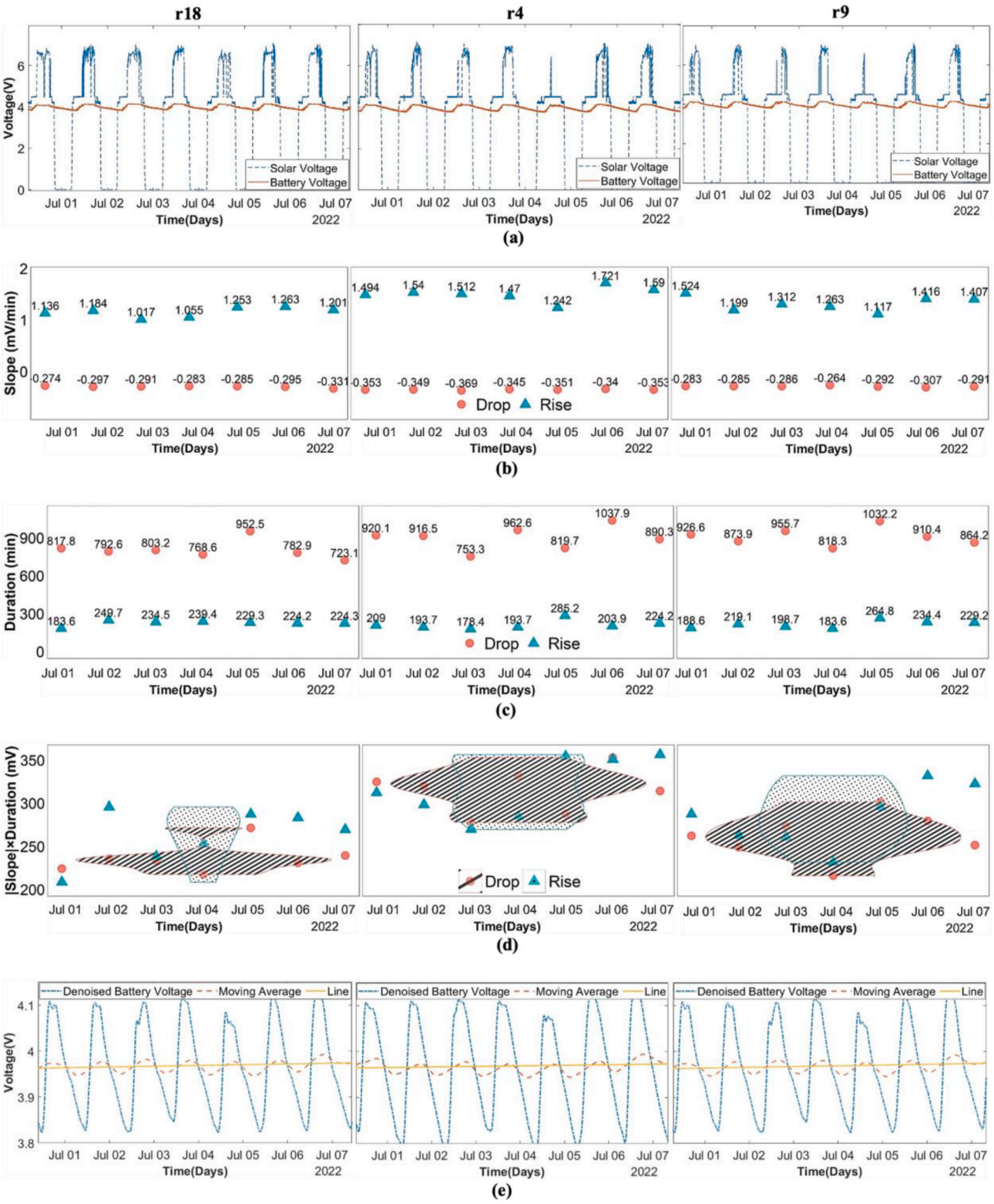

Fig. 14. Results of the voltage analysis for the rain sensors during the first week of July (a) voltage graphs (b) slop data (c) duration data (d) |slop| × duration data (e) voltage trend of change.

online interface. Fig. 11 shows the schematic illustration of the deployment process of a sonar sensor. First, a sign and a stand were fixed to the ground. Next, the assembled sensor node and its energy circuit were attached to the stand. A hotspot, its battery, and a charge controller were positioned inside a box and the 25W solar panel was placed adjacent to the box. Lastly, the researchers verified wireless connectivity between the sensor, the hotspot, and the user interface using a laptop.

To address the imperfections of solar-based energy harvesting because of daylighting variations, the researchers deployed solar panels toward the south with tilt angles between 0 and 45° that is approximately the latitude of the locations plus 15°.These range and direction are recommended by the US National Renewable Energy Laboratory

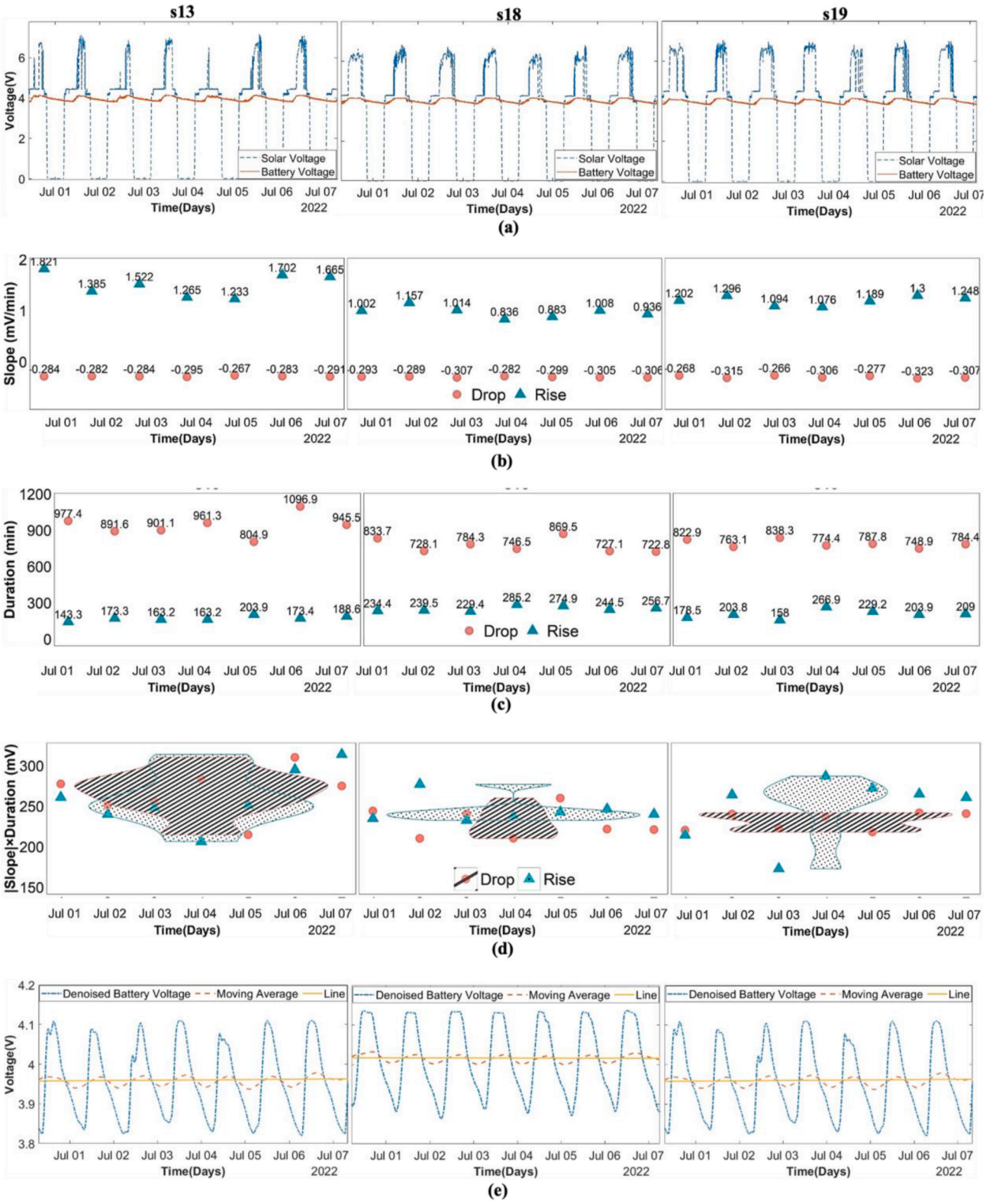

Fig. 15. Results of the voltage analysis for the sonar sensors (a) voltage graphs (b) slop data (c) duration data (d) |slop| × duration data (e) voltage trend of change.

(NREL) for capturing the highest average yearly solar radiation (Dunlap et al., 1994) when utilizing flat panels. Additionally, the panels were positioned in locations under no or negligible shading conditions to achieve maximum possible sunlight. To tackle the imperfections of solar-based energy harvesting caused by weather variations especially preventing the battery charge drop because of low temperature effect, the research group designed a winter isolation system for the deployed batteries including the 3.7V lithium-polymer batteries of the sensor nodes, the 12V lead acid batteries of the communication nodes, and the hotspots. Additionally, the boxes' design including their size and natural ventilation prevented overheating of the electric devices inside them during the field deployment.

Table 5
Summary of the evaluation results.

Day	Rain						Sonar					
	r4		r9		r18		s13		s18		s19	
	Voltage Rise (mV)	Voltage Drop (mV)	Voltage Rise (mV)	Voltage Drop (mV)	Voltage Rise (mV)	Voltage Drop (mV)	Voltage Rise (mV)	Voltage Drop (mV)	Voltage Rise (mV)	Voltage Drop (mV)	Voltage Rise (mV)	Voltage Drop (mV)
Jun 30	312.23	−324.8	287.48	−262.22	208.53	−224.09	260.98	−277.59	234.9	−244.26	214.51	−220.55
Jul 1	298.23	−319.9	262.74	−249.05	295.63	−235.41	240.04	−251.44	277.12	−210.43	264.17	−240.39
Jul 2	269.74	−278	260.76	−273.33	238.44	−233.73	248.39	−255.9	232.58	−240.77	172.88	−222.98
Jul 3	284.79	−332.1	231.83	−216.02	252.59	−217.5	206.45	−283.57	238.46	−210.51	287.14	−236.98
Jul 4	354.2	−287.7	295.8	−301.41	287.34	−271.47	251.43	−214.92	242.73	−259.99	272.49	−218.23
Jul 5	350.83	−352.9	331.93	−279.49	283.15	−230.95	295.07	−310.42	246.41	−221.77	265.09	−241.89
Jul 6	356.43	−314.3	322.51	−251.49	269.34	−239.36	313.96	−275.13	240.31	−221.17	260.78	−240.82
Sum	2227	−2210	1993	−1833	1835	−1653	1816	−1869	1713	−1609	1737	−1622

4. Results and assessments

The sensor readings are saved on a server database and then are plotted on the GUI which together constitute the user interface of the sensor system. Because the data presented for assessing the sensors are achieved from this frontend, this section first describes the user interface. Next, it explains the approach used for automating voltage evaluation and then explores the graphs of the batteries and solar panel's voltages for some sensor nodes. Afterwards, the voltage variations in communication nodes' batteries are discussed and finally the uptime and downtime of 54 sensors including 26 sonar sensors, 20 rain sensors and 8 temperature/humidity sensors are presented and analyzed for one month. These findings provide insights into the effectiveness of the designed energy circuits and the system's overall reliability.

4.1. User interface

The user interface includes two main elements: (1) a Structured Query Language (SQL) database with limited access (Mohammadkhorasani et al., 2023) and (2) an open-access internet website implemented in JavaScript. The SQL database stores any data collected by the sensor network and provides a means for high-level non-real-time data analysis. Whereas the website acquires the recent data from the database, retains it for a limited time, conducts noncomplex processing and presents the data in a graph format. The transmission interval from the sensors is currently every 30s but data-transfer from sensor to the database and from the database to the website is in real-time. Furthermore, the data processing and demonstration within the java scripts of the website is performed in real-time. Therefore, the update time of the website in the current format is approximately 30s.

Fig. 12 shows the website and describes its basic elements. In its homepage, the website provides the access buttons to each deployment location as demonstrated in Fig. 12a. The designation of the sensors at different locations are demonstrated with different colors on the homepage but access to individual sensors is through the location buttons. Each color represents a condition: blue sensors have unimpededly functioned for more than a week; green represents the sensors that have worked for 48hr to one week without disconnection, orange sensors have operated for less than 2hrs; and red sensors are disconnected. A location page provides the access buttons to every sensor in that location and gives some information on the condition of each sensor and communication node as depicted in Fig. 12b.The user can access the collected data using sensors' access buttons through which plots of the latest update of the sensors' measurements are presented. Fig. 12c shows an example of collected data of rain by sensor r4 from the website. Additionally, the voltages of solar panels and batteries are updated every 30s on the website offering a means for sensors' energy monitoring in near-real-time.

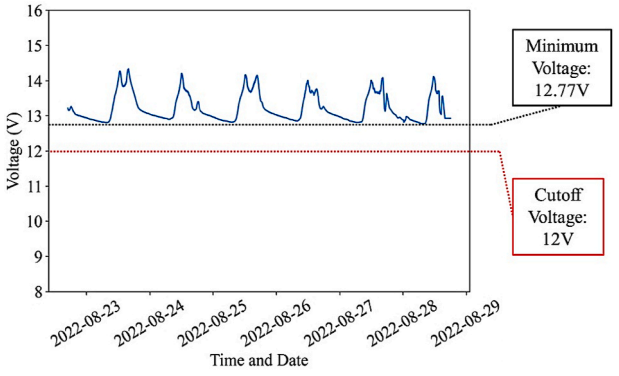

Fig. 16. Validation in the voltage of the communication nodes' batteries.

4.2. Automated voltage analysis

The discharge cutoff voltage of the sensor nodes' batteries is 3.0V as shown in Fig. 2. Reducing the voltages beyond this level is harmful for the batteries thus it is required they remain above this limit during normal operation (Kuo et al., 2016). However, the voltage will not fall beyond the cutoff level if the increase in voltage during charging is capable of compensating for the decrease during discharge. Therefore, the assessment criterion specified for the sustainability of the sensor nodes in this study is the direction of change in the voltages of the sensor. Specifically, the slope and duration of voltage drop/rise are analyzed for a period of in-field operation through which the overall trend is calculated.

Fig. 13 describes the employed method to calculate the slope and duration of drop and rise in the batteries' voltages using an exemplary sensor deployed at the Three Sister location in Ohkay Owingeh. The battery and solar panel voltage data in Fig. 13a is acquired from the user interface. Fig. 13a also shows the linear approximation of the mentioned slopes and durations for that sensor. This approximation requires estimation of the start as well as the end of the charge and discharge processes. Fig. 13b signifies those starts and ends with four letters: A and B are the start and end of the charge process, while C and D are the start and the end of the discharge process. This study uses a supervised Machine Learning (ML) approach to automatically detect these points during charge and discharge and subsequently computes the mentioned slopes and durations. Five classes for voltage data are defined as described in Fig. 13c and the data of several sensors are accordingly tagged for training the model. The features used in the ML model include the slopes of the lines starting from the point of interest and ending at different increments. Different classification techniques are employed and tested with diverse test-sets to identify a model with the desired accuracy, in turn, an ensemble learner with discriminant classifier is

used to extract the start of charge (A) and the end of charge and discharge processes (B and D, respectively) as shown in Fig. 13d. This classifier, however, fails to detect the start of discharge (C), thus, a second model with the same classifier but with optimized hyper-parameters are employed as shown in Fig. 13e. Finally, an algorithm based on the pattern of the class variation in the second model detects the start of the discharge process and subsequently calculates the slopes and durations. MATLAB was utilized for training and parameter identification of the ML model, the classification implementation, and the computation of the voltage slopes.

The results show that if the batteries' initial voltage is above 4.1V, the designed energy circuit described in Fig. 2 can provide power for them to operate above their cutoff voltage for one week in remote locations. For example, one-week evaluation of the rain sensors in Fig. 14 shows that the minimum voltage of r4, r9, and r18 are 3.78V, 3.82V, and 3.84V. These minimum voltage levels exceed 3V that is the discharge cutoff voltage of the sensor nodes' batteries in Fig. 2. Additionally, as it is shown in Fig. 15, the sonar voltage assessment during the first week of July demonstrates that s13, s18, and s19 have a minimum voltage of 3.82V, 3.88V, and 3.84V, respectively. Therefore, the consumption of the sonar sensors does not cause the batteries to get lower than the cutoff voltage in the designed energy system in summer and fall, proving that the design fulfils the assessment criterion specified for the sustainability of the sensor nodes in this study. It should be noted that some batteries went off during the experiment, but the energy insufficiency was not the major reason. Table 5 provides a summary of the power evaluation results, illustrating the disparity between the drop and rise in battery voltage of the sensor node over the evaluation period. The table affirms that the voltage drops, and rises are closely aligned; however, it is noteworthy that, among the six evaluated sensors, the rise in voltage surpasses the voltage drop for five of them.

4.3. Voltage sufficiency in communication nodes

Fig. 16 shows the variations in the voltage of the battery used to charge a hotspot from August 22 to August 29, 2022. The measured voltage stands above the battery cutoff voltage by a margin. This margin, which is always equal or higher than 0.77V during this measurement offers a safety factor of 1.064 for the voltage of hotspot battery. Likewise, upon visual inspection of the voltage graph the voltage does not follow a downward trend. Accordingly, the design of energy system of the communication nodes satisfies the voltage criterion imposed by the battery cutoff voltage.

4.4. Result summary

Fig. 17 provides a summary of the experimental deployment of the rain and sonar sensors in the network from September 20th to October 20th, 2022, indicating their online and outage intervals. The uptimes of sonar and rain sensors are represented by blue and green colors, respectively. Additionally, the node sensors including the communication nodes, plus a thermometer and a humidity sensor per each node are shown with red color in this figure. Moreover, the white areas represent the downtimes of the sensors, that are the failures in real-time data

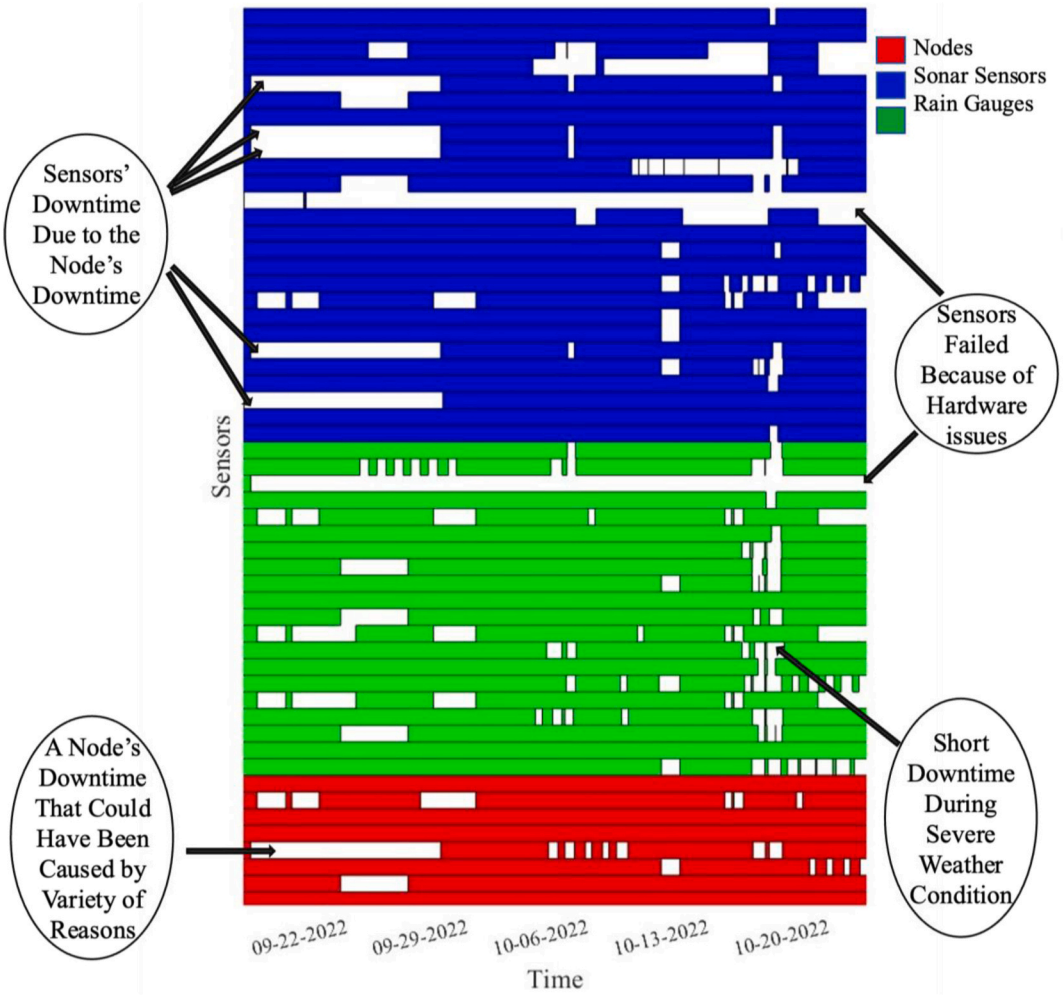

Fig. 17. Experimental evaluation's summary of the rain, sonar, and node (temperature and humidity) sensors.

acquisition by the sensors caused by variety of reasons. The failures in communication nodes caused by different factors such as lack of network, hotspots' battery depletion, surpassing the allowable temperature range accounts for most of the downtimes of the sensors in the network. Additionally, hardware problems result in the permanent failure of some of the sensors. Severe weather conditions are another factor causing short- or long-term downtime of the sensors. Usually, these sensors automatically restore power and resume operations after heavy rains or strong winds. However, in some cases, maintenance is required to bring them back to full functionality. Most of the sensors in Fig. 17 are operational throughout the graph with occasional disruptions due to severe weather conditions and some maintenance issues. The rain and node sensors exhibit a higher level of reliability than the sonar sensors, which experiences more frequent downtime due to battery depletion and signal interference. Nevertheless, the network achieves a satisfactory operation in its level of coverage and sustainability in detecting precipitation and water level changes, demonstrating the potential of such sensor systems for monitoring environmental conditions and informing sustainable low-cost flood prediction strategies.

5. Conclusion

This study presents a solar energy system for a WSSN collecting data in remote regions. The proposed system, a sensor network composed of several water level and rain sensors, connected via communication nodes were validated through a deployment across several remote areas of Ohkay Owingeh. In its duration, a real-time voltage monitoring network recorded copious amounts of energy data to provide the design validation. The variations in the voltage of solar panels and the batteries of several sensors are monitored and analyzed using an ensemble learning model with a discriminant classifier in MATLAB. The results show the power consumption of the sensor nodes does not cause the batteries to fall behind the discharge cutoff voltage. Ergo, the design fulfils the assessment criterion specified for voltage sufficiency and the proposed energy system shows power sustainability for the sensor operation in summer. The efficiency of solar systems, however, relies on different environmental factors such as the sun angle, daytime length and the ambient weather which varies on a seasonal basis. Hence, a possible future area of investigation is to test the proposed system during other seasons to validate the design with higher certainty.

Declaration of competing interest

The authors declare that they have no known competing financial interests or personal relationships that could have appeared to influence the work reported in this paper.

Acknowledgement

This work is funded by the National Science Foundation (NSF), Division of Computer and Network Systems (CNS), Directory for Computer and Information Science and Engineering (CISE), Smart and Connected Communities, CIVIL Challenge, Grant/Award Number: 2133334; and NSF Division of Information & Intelligent Systems (IIS) CISE, Hardening the Data Revolution DSC, Grant/Award Number: 2123346. The authors also thank Marlan Ball, John-Wesley Hanson, Daniel Gavin, Tim Thiegart, and Dalton Deberry for their invaluable technical contributions to this study, and the leadership and assistance from Sreenivas Alampalli (Stantec); and Phoebe Suina, Tom Teegarden (High Water Mark, LLC). The authors recognize the support from the Pueblo of Ohkay Owingeh for granting us permission to using their lands as part of this project and their involvement in selecting sites and providing input in the hardware and software of the LEWIS system, data collection, and sensor locations.

References

Afzal, M.I., Mahmood, W., Akbar, A.H., 2008. A battery recharge model for wsns using free-space optics (FSO). In: 2008 IEEE International Multitopic Conference. IEEE, pp. 272–277. https://doi.org/10.1109/INMIC.2008.4777748.

Akhtar, F., Rehmani, M.H., 2015. Energy replenishment using renewable and traditional energy resources for sustainable wireless sensor networks: a review. Renew. Sustain. Energy Rev. 45, 769–784. https://doi.org/10.1016/j.rser.2015.02.021.

Andringa, M.M., Neikirk, D.P., Dickerson, N.P., Wood, S.L., 2005. Unpowered wireless corrosion sensor for steel reinforced concrete. In: Sensors, 2005 IEEE. IEEE, p. 4. https://doi.org/10.1109/ICSENS.2005.1597659.

Aris, A.M., Shabani, B., 2017. An experimental study of a lithium ion cell operation at low temperature conditions. Energy Proc. 110, 128–135. https://doi.org/10.1016/j.egypro.2017.03.117.

Barrenetxea, G., Ingelrest, F., Schaefer, G., Vetterli, M., 2008. The hitchhiker's guide to successful wireless sensor network deployments. In: Proceedings of the 6th ACM Conference on Embedded Network Sensor Systems, pp. 43–56. https://doi.org/10.1145/1460412.1460418.

Botero-Valencia, J.S., Mejia-Herrera, M., Pearce, J.M., 2022. Low cost climate station for smart agriculture applications with photovoltaic energy and wireless communication. HardwareX 11, e00296. https://doi.org/10.1016/j.ohx.2022.e00296.

Candia, A., Represa, S.N., Giuliani, D., Luengo, M.Á., Porta, A.A., Marrone, L.A., 2018. Solutions for SmartCities: proposal of a monitoring system of air quality based on a LoRaWAN network with low-cost sensors. In: 2018 CACIDI. IEEE, pp. 1–6. https://doi.org/10.1109/CACIDI.2018.8584183.

Corke, P., Valencia, P., Sikka, P., Wark, T., Overs, L., 2007. Long-duration solar-powered wireless sensor networks. In: Proceedings of the 4th Workshop on Embedded Networked Sensors, pp. 33–37. https://doi.org/10.1145/1278972.1278980.

Dehwah, A.H., Mousa, M., Claudel, C.G., 2015. Lessons learned on solar powered wireless sensor network deployments in urban, desert environments. Ad Hoc Netw. 28, 52–67. https://doi.org/10.1016/j.adhoc.2015.01.013.

Denisov, A., Yeatman, E., 2010. Ultrasonic vs. inductive power delivery for miniature biomedical implants. In: 2010 International Conference on Body Sensor Networks. IEEE, pp. 84–89. https://doi.org/10.1109/BSN.2010.27.

Dunlap, M.A., Marion, W., Wilcox, S., 1994. Solar Radiation Data Manual for Flat-plate and Concentrating Collectors (No. NREL/TP-463-5607). NREL, Golden, CO (United States). https://doi.org/10.2172/10169141.

Dutta, P., Hui, J., Jeong, J., Kim, S., Sharp, C., Taneja, J., et al., 2006. Trio: enabling sustainable and scalable outdoor wireless sensor network deployments. In: Proceedings of the 5th International Conference on Information Processing in Sensor Networks, pp. 407–415. https://doi.org/10.1145/1127777.1127839.

Getahun, M., Azath, M., Sharma, D.P., Tuni, A., Adane, A., 2022. Efficient energy utilization algorithm through energy harvesting for heterogeneous clustered wireless sensor network. Wireless Commun. Mobile Comput. 2022 https://doi.org/10.1155/2022/4154742.

Goudar, V., Ren, Z., Brochu, P., Potkonjak, M., Pei, Q., 2013. Optimizing the output of a human-powered energy harvesting system with miniaturization and integrated control. IEEE Sensor. J. 14 (7), 2084–2091. https://doi.org/10.1109/JSEN.2013.2290738.

Guo, D., Shan, M., Owusu, E.K., 2021. Resilience assessment frameworks of critical infrastructures: state-of-the-art review. Buildings 11 (10), 464. https://doi.org/10.3390/buildings11100464.

Jackson, G., Ciocoiu, S., McCann, J.A., 2017. Solar energy harvesting optimization for wireless sensor networks. In: GLOBECOM 2017-2017 IEEE Global Communications Conference. IEEE, pp. 1–6. https://doi.org/10.1109/GLOCOM.2017.8254851.

Karagulian, F., Barbiere, M., Kotsev, A., Spinelle, L., Gerboles, M., Lagler, F., Borowiak, A., 2019. Review of the performance of low-cost sensors for air quality monitoring. Atmosphere 10 (9), 506. https://doi.org/10.3390/atmos10090506.

Khandelwal, D.D., Singhal, M., 2021. Developing a low-cost weather monitoring system for data-sparse regions of the Himalayas. Weather 76 (2), 60–64. https://doi.org/10.1002/wea.3647.

Kuo, T.J., Lee, K.Y., Huang, C.K., Chen, J.H., Chiu, W.L., Huang, C.F., Wu, S.D., 2016. State of charge modeling of lithium-ion batteries using dual exponential functions. J. Power Sources 315, 331–338. https://doi.org/10.1016/j.jpowsour.2016.03.021.

LaMarca, A., Brunette, W., Koizumi, D., Lease, M., Sigurdsson, S.B., Sikorski, K., Borriello, G., 2002. Making sensor networks practical with robots. In: Pervasive Computing: First International Conference, Pervasive 2002 Zurich, Switzerland, 2002 Proceedings 1. Springer Berlin Heidelberg, pp. 152–166. https://doi.org/10.1007/3-540-45866-2_13.

Li, P., 2008. Energy storage is the core of renewable technologies. IEEE Nanotechnol. Mag. 2 (4), 13–18. https://doi.org/10.1109/MNANO.2009.932032.

LokeshReddy, M., Kumar, P.P., Chandra, S.A.M., Babu, T.S., Rajasekar, N., 2017. Comparative study on charge controller techniques for solar PV system. Energy Proc. 117, 1070–1077. https://doi.org/10.1016/j.egypro.2017.05.230.

Ma, M., He, B., Wang, N., Shen, R., 2022. A method for monitoring the solar resources of high-scale photovoltaic power plants based on wireless sensor networks. Sustain. Energy Technol. Assess. 53, 102678 https://doi.org/10.1016/j.seta.2022.102678.

Ma, Z., Choi, J., Sohn, H., 2023. Structural displacement sensing techniques for civil infrastructure: a review. J. Infrastruct. Intell. Resilience 2 (3), 100041. https://doi.org/10.1016/j.iintel.2023.100041.

Mansura, A., Drieberg, M., Aziz, A.A., Bassoo, V., Sarang, S., 2022. An energy balanced and nodes aware routing protocol for energy harvesting wireless sensor networks. Peer-to-Peer Netw. Appl. 15 (2), 1255–1280. https://doi.org/10.1007/s12083-022-01292-w.

Mao, F., Khamis, K., Krause, S., Clark, J., Hannah, D.M., 2019. Low-cost environmental sensor networks: recent advances and future directions. Front. Earth Sci. 7, 221. https://doi.org/10.3389/feart.2019.00221.

Marion, B., Anderberg, M., Gray-Hann, P., 2005. Recent Revisions to PVWATTS (No. NREL/CP-520-38975). NREL, Golden, CO (United States). https://www.osti.gov/servlets/purl/882800.

Misol, 2022. Spare Part for Weather Station to Measure the Rain Volume, for Rain Meter, for Rain Gauge. Available from. www.misolie.net.

Mohammadkhorasani, A., Malek, K., Mojidra, R., Li, J., Bennett, C., Collins, W., Moreu, F., 2023. Augmented reality-computer vision combination for automatic fatigue crack detection and localization. Comput. Ind. 149, 103936 https://doi.org/10.1016/j.compind.2023.103936.

Mottahedi, A., Sereshki, F., Ataei, M., Nouri Qarahasanlou, A., Barabadi, A., 2021. The resilience of critical infrastructure systems: a systematic literature review. Energies 14 (6), 1571. https://doi.org/10.3390/en14061571.

Naser, M.Z., 2023. Machine learning for all! Benchmarking automated, explainable, and coding-free platforms on civil and environmental engineering problems. J. Infrastruct. Intell. Resilience 2 (1), 100028. https://doi.org/10.1016/j.iintel.2023.100028.

Naseri, K., Hummel, M., 2021. Development of a Bayesian Copula-based nonstationary framework for compound flood risk assessment. In: AGU Fall Meeting Abstracts, vol. 2021 p. NH15D-0471).

Nsabagwa, M., Byamukama, M., Kondela, E., Otim, J.S., 2019. Towards a robust and affordable automatic weather station. Dev. Eng. 4, 100040 https://doi.org/10.1016/j.deveng.2018.100040.

Ozdagli, A.I., Liu, B., Moreu, F., 2018. Low-cost, efficient wireless intelligent sensors (LEWIS) measuring real-time reference-free dynamic displacements. Mech. Syst. Signal Process. 107, 343–356. https://doi.org/10.1016/j.ymssp.2018.01.034.

Ozeri, S., Shmilovitz, D., 2010. Ultrasonic transcutaneous energy transfer for powering implanted devices. Ultrasonics 50 (6), 556–566. https://doi.org/10.1016/j.ultras.2009.11.004.

Roundy, S., Wright, P.K., 2004. A piezoelectric vibration based generator for wireless electronics. Smart Mater. Struct. 13 (5), 1131. https://doi.org/10.1088/0964-1726/13/5/018.

Sardini, E., Serpelloni, M., 2010. Self-powered wireless sensor for air temperature and velocity measurements with energy harvesting capability. IEEE Trans. Instrum. Meas. 60 (5), 1838–1844. https://doi.org/10.1109/TIM.2010.2089090.

Savina, M., Schäppi, B., Molnar, P., Burlando, P., Sevruk, B., 2012. Comparison of a tipping-bucket and electronic weighing precipitation gage for snowfall. Atmos. Res. 103, 45–51. https://doi.org/10.1016/j.atmosres.2011.06.010.

Shanmuganthan, S., Ghobakhlou, A., Sallis, P., 2008. Sensor data acquisition for climate change modelling. WSEAS Trans. Circuits Syst. 7 (11), 942–952.

Sharma, H., Haque, A., Jaffery, Z.A., 2018. An efficient solar energy harvesting system for wireless sensor nodes. In: 2018 2nd IEEE ICPEICES. IEEE, pp. 461–464. https://doi.org/10.1109/ICPEICES.2018.8897434.

Shen, L., Wang, H., Duan, X., Li, X., 2008. Application of wireless sensor networks in the prediction of wind power generation. In: 2008 4th International Conference on Wireless Communications, Networking and Mobile Computing. IEEE, pp. 1–4. https://doi.org/10.1109/WiCom.2008.959.

Simjee, F., Chou, P.H., 2006. Everlast: long-life, supercapacitor-operated wireless sensor node. In: Proceedings of the 2006 International Symposium on Low Power Electronics and Design, pp. 197–202. https://doi.org/10.1145/1165573.1165619.

Wan, J., Chen, J., 2022. AHP based relay selection strategy for energy harvesting wireless sensor networks. Future Generat. Comput. Syst. 128, 36–44. https://doi.org/10.1016/j.future.2021.09.038.

Wang, Z.L., Song, J., 2006. Piezoelectric nanogenerators based on zinc oxide nanowire arrays. Science 312 (5771), 242–246. https://doi.org/10.1126/science.1124005.

Wang, C., Li, J., Yang, Y., Ye, F., 2017. Combining solar energy harvesting with wireless charging for hybrid wireless sensor networks. IEEE Trans. Mobile Comput. 17 (3), 560–576. https://doi.org/10.1109/TMC.2017.2732979.

Waterston, J., Rhea, J., Peterson, S., Bolick, L., Ayers, J., Ellen, J., 2019. Ocean of things: affordable maritime sensors with scalable analysis. In: OCEANS 2019-Marseille. IEEE, pp. 1–6. https://doi.org/10.1109/OCEANSE.2019.8867398.

Weimer, M.A., Paing, T.S., Zane, R.A., 2006. Remote area wind energy harvesting for low-power autonomous sensors. In: 2006 37th IEEE Power Electronics Specialists Conference. IEEE, pp. 1–5. https://doi.org/10.1109/pesc.2006.1712213.

Xiao, X., Wang, M., Cao, G., 2023. Solar energy harvesting and wireless charging based temperature monitoring system for food storage. Sens. Int. 4, 100208 https://doi.org/10.1016/j.sintl.2022.100208.

Yang, F., Shu, L., Huang, K., Li, K., Han, G., Liu, Y., 2020. A partition-based node deployment strategy in solar insecticidal lamps Internet of Things. IEEE Internet Things J. 7 (11), 11223–11237. https://doi.org/10.1109/JIOT.2020.2996514.

Yao, W., Li, M., Wu, M.Y., 2006. Inductive charging with multiple charger nodes in wireless sensor networks. In: Advanced Web and Network Technologies, and Applications: APWeb 2006 International Workshops: XRA, IWSN, MEGA, and ICSE, Harbin, China, January 16-18, 2006. Proceedings 8. Springer Berlin Heidelberg, pp. 262–270. https://doi.org/10.1007/11610496_34.

Zakaria, M.I., Jabbar, W.A., Sulaiman, N., 2023. Development of a smart sensing unit for LoRaWAN-based IoT flood monitoring and warning system in catchment areas. Internet Things Cyber-Phys. Syst. 3, 249–261. https://doi.org/10.1016/j.iotcps.2023.04.005.